ORGANIC CHEMISTRY FRONTIERS

RESEARCH ARTICLE

View Article Online
View Journal

Cite this: DOI: 10.1039/d6qo00267f

Enabling C–C bond-forming strategies for tailored derivatisation of heptazine frameworks

Aurélien Huet, Benjamin Louis, Rana Deeba, Ahmed Ait Khouya, Yves Chenavier, Renaud Demadrille, Jacques Pécaut, Lionel Dubois* and Julie Andrez*

Received 3rd March 2026,
Accepted 19th March 2026

DOI: 10.1039/d6qo00267f

rsc.li/frontiers-organic

Interest in melon-related graphitic carbon nitride (g-CN) materials has recently increased significantly due to their appealing properties as metal-free photocatalysts. Heptazine derivatives are now used in a variety of applications, including photocatalysis, organic light-emitting diodes (OLEDs), sensors, gas separation and lithium-ion batteries. However, the chemistry and functionalisation of these materials have been limited due to the difficulty of controlling the reactivity of the heptazine core. This study presents a comprehensive analysis of previously inaccessible C–C coupling reactions, including the Suzuki, Sonogashira, Stille, Kumada and Negishi reactions, which have been successfully applied to dialkylamine-substituted heptazines. These advances establish a robust platform for the derivatisation of a broader range of heptazines. Particular emphasis is placed on the Stille reaction, demonstrating the influence of aryl electronic effects on yields. The electron-withdrawing nature of the heptazine core was further confirmed by evaluating subsequent post-functionalisation (nitration, bromination, and a second Stille coupling) on selected substituted heptazines. Electrochemical (CV) and optical (UV-Vis absorption/emission) studies demonstrate a clear dependence of the electronic properties on the substituent. Overall, these findings deepen our understanding of the relationships between the structure and properties of heptazine materials, providing guidance for their targeted molecular design.

Introduction

Heptazine is an emerging building block for developing efficient organic and composite materials for use in energy conversion. Since Antonietti *et al.* discovered the photocatalytic properties of g-CN,[1] a heptazine-based polymer, for the hydrogen evolution reaction (HER), extensive research has been conducted to study the (photo)catalytic properties of polymers, oligomers and simple molecules based on heptazine. Reactions of interest include H_2O_2 production,[2] water splitting,[3] CO_2 reduction,[4,5] and N_2 fixation[6] and reduction.[7] Heptazine-based compounds are also used in the design of OLEDs,[8–11] MOFs and COFs with applications in sensors,[12,13] gas separation[14] or Li-ion batteries.[15] The important point is that heptazine and its derivatives have interesting properties as photosensitizers, catalysts and catalyst supports. The catalytic and physicochemical properties of heptazine-based materials are closely linked to the functionalisation of the three positions available on the heptazine synthon. This highlights the crucial importance of mastering heptazine chemistry.[8,16] This chemistry is based on the high stability of the heptazine moiety. Access to heptazine compounds relies on the pyrolysis of nitrogen-rich molecules at high temperature (>500 °C), which leads to the formation of heptazine-tris-amino (melem) polymers (see Fig. 1). The melem monomer can be treated with hydrazine to produce tri-pyrazolyl heptazine.[17] The polymers can then be hydrolysed and further halogenated to obtain tri-chloro heptazine (**Hept-Cl$_3$**)[18] or the lesser known tri-bromo heptazine (**Hept-Br$_3$**).[19] Although promising, **Hepta-Br$_3$** has never been used as a starting building block in heptazine functionalisation, despite having been described. Currently, **Hepta-Cl$_3$**, tri-pyrazolyl and tri-pyrrolyl heptazines are the only entry points into all the known heptazine chemistry,[17,18,20] and the successful reactions to functionalise these heptazine synthons have been limited. Classical nucleophilic substitution can lead to a family of symmetric heteroatom-substituted heptazines.[18,21–26] Examples of dissymmetrically substituted heptazines (C_s symmetry) are rare and are limited to amines.[27–29] With the exception of Friedel–Crafts arylation (and the limitations implied by the directing group),[30–33] electrophilic substitution reactions and C–C couplings have been unsuccessful with **Hepta-Cl$_3$** so far.

Interestingly, a recent study by Mayder *et al.* demonstrated the feasibility of Negishi coupling to produce a three carbazole-substituted heptazine, albeit with a modest yield of 21%.[34] This exciting result prompted us to reinvestigate the C–

Univ. Grenoble Alpes, CEA, CNRS, IRIG-SyMMES (UMR5819), 38000 Grenoble, France. E-mail: Julie.andrez@cea.fr, lionel.dubois@cea.fr

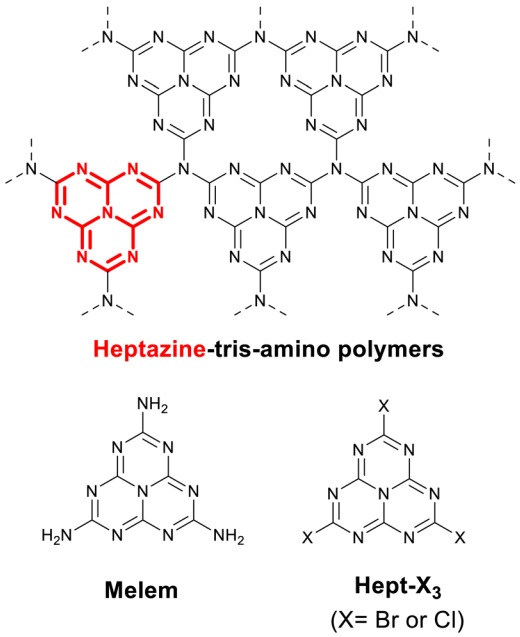

Fig. 1 Schematic representation of heptazine derivatives: heptazine polymers (g-CN), melem and tri-halogeno heptazine (**Hept-X$_3$**).

C functionalisation capabilities of halogeno-heptazines. In order to restrict the C–C coupling reaction to a single position, we focused our studies on mono-bromo- and mono-chloro heptazines.

Thanks to the use of dissymmetrical mono-halogeno heptazine, we report five types of successful C–C coupling reactions on the heptazine platform under classical conditions (Suzuki, Sonogashira, Stille, Kumada and Negishi reactions). The first four of these are unprecedented in the literature and enable the novel functionalisation of the heptazine scaffold. With a focus on the Stille reaction, we studied the impact of different types of substituents with various electronic properties on the outcome of the coupling reaction. Thanks to the newly developed functionalisation chemistry, we demonstrate that the electronic and optical properties of heptazine derivatives can be finely tuned, providing fundamental insights that will be helpful for future molecule design in diverse fields such as photocatalysis,[7,35–38] OLEDs,[8–11] sensors,[12,13] gas separation[14] or Li-ion batteries.[15]

Results and discussion

Newly accessible C–C couplings

We synthesized the little known **Hepta-Br$_3$** using an adapted procedure involving the reaction of potassium cyamelurate in a sealed vessel with PBr_5 formed *in situ*.[19] Subsequent sublimation of the crude product afforded **Hepta-Br$_3$** in 55% yield. The ^{13}C NMR spectrum (Fig. S1) is consistent with that previously reported. In addition, single crystals suitable for X-ray diffraction were grown by slow cooling of a saturated toluene solution of **Hepta-Br$_3$** under argon. The crystal structure

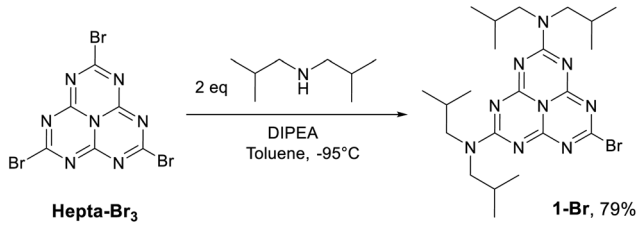

Scheme 1 Synthesis of the starting compound **1-Br**.

(Fig. S151) is identical to the trichloro-*s*-heptazine structure reported by Kroke *et al.* in 2002 in terms of C–N bonds and angles.[18] As expected, only the C–Br bonds are longer (averaging 1.875(2) Å) than the C–Cl bonds (averaging 1.716(4) Å).

With the dual objective of restricting the C–C coupling reactions to a single position and improving the solubility properties of both starting materials and final products in organic solvents, **Hepta-Br$_3$** was first disubstituted with two equivalents of diisobutylamine. Following a protocol previously reported by our group with the chloride analogue,[29] we selectively obtained the monobromide compound **1-Br** in 79% yield (Scheme 1). It should be noted that this substitution by diisobutylamine also modifies the electronic properties of the heptazine bromide, making **1-Br** more electron-rich than **Hepta-Br$_3$**. This could influence its reactivity towards C–C coupling reactions. Compound **1-Br** was characterised using ^{1}H NMR, ^{13}C NMR, FTIR, mass spectrometry and single crystal X-ray diffraction analyses (see the SI). Five different palladium-catalysed cross-couplings, starting from **1-Br**, were tested under their respective classical conditions involving aromatic substituents and classical organic fragments in C–C coupling reactions.[39] Indeed, unsaturated substrates undergo coupling more easily, notably due to the catalyst's ability to facilitate this process. Excellent yields were obtained for these five types of reactions, calculated from the purified and isolated products (see Scheme 2). The triphenylamine heptazine derivative **2** was obtained in 82% yield from the Suzuki coupling of **1-Br** and 4-(diphenylamino)phenylboronic acid pinacol ester. The Sonogashira coupling of **1-Br** and phenylacetylene results in the formation of the novel heptazine compound **3** in 67% yield. The new thienyl heptazine derivative **4** was obtained by Negishi and Suzuki coupling of **1-Br** and the thienyl organozinc and the thienylboronic ester, respectively, in yields of 69% and 79%. The phenyl heptazine compound **5** was synthesised *via* both Stille and Kumada coupling reactions using **1-Br** and a phenyl organostannane or phenyl Grignard reagent, respectively, with no significant impact on the yield of the reaction (86 and 73%, respectively). A *para*-anisolyl heptazine derivative **6** was obtained in 78% yield from the Stille coupling of **1-Br** and the preformed anisolyl organostannane. The compounds **2–6** were characterised using NMR (^{1}H, ^{13}C and 2D techniques), mass spectrometry and FTIR spectroscopy (see the SI). All analyses converge to validate the structure of each molecule. Notably, the FTIR spectrum of **3** shows a characteristic peak at 2230 cm^{-1}, assigned to disubstituted C≡C stretching

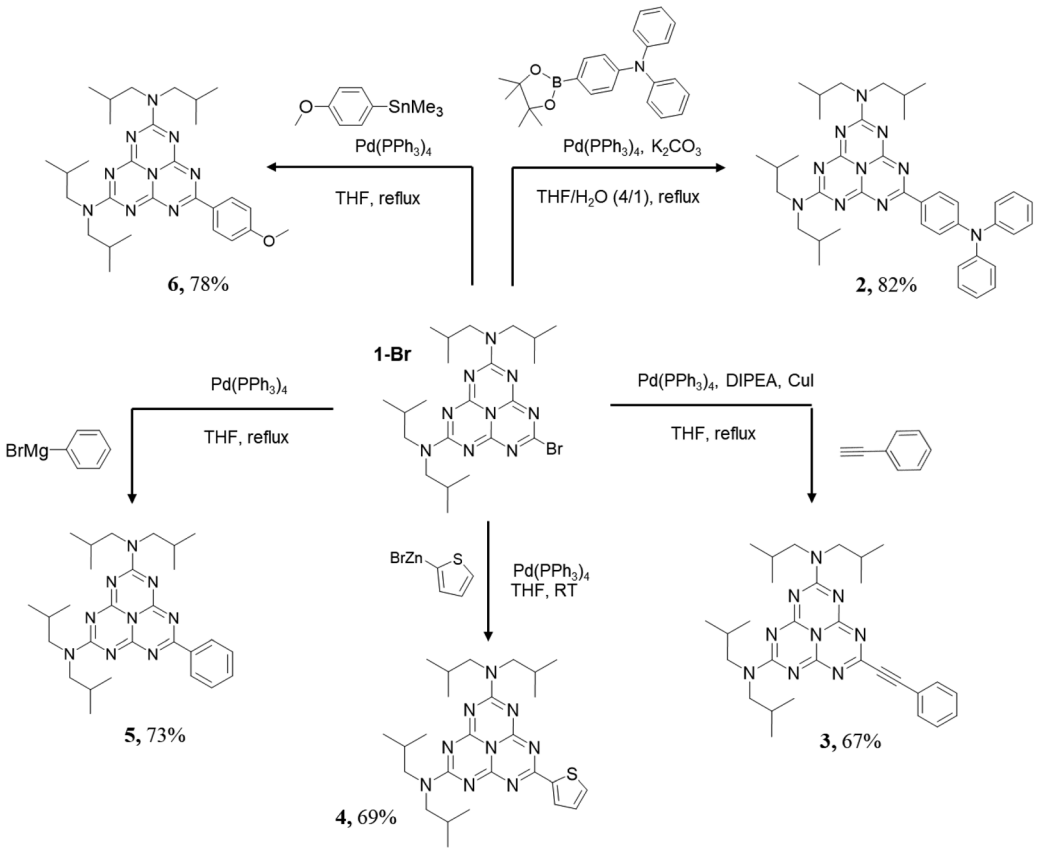

Scheme 2 Examples of the C–C coupling reaction achieved on heptazine derivative **1-Br**.

vibrations. It should be noted that such classical functionalisation reactions were previously considered unattainable for heptazine derivatives. The success of these cross-coupling reactions is not dependent on the halogen nature of compound **1-Br** as the chloride analogue **1-Cl** also led to compounds **2** and **3** in 73% and 65% yields, respectively, *via* Suzuki and Sonogashira coupling under the same conditions. The strong electron-withdrawing properties of the heptazine moiety make compound **1-Cl** more reactive than classical aromatic chlorides, particularly during the oxidative addition on electron-rich Pd^0 in Stille coupling reactions.[40,41] The fact that such well-known coupling reactions have not yet been reported (or only with modest yield[34]) with heptazine derivatives is probably because **Hepta-Cl$_3$** was used as the starting material in an attempt to perform three successive C–C couplings. **Hepta-X$_3$** is a more reactive and sensitive compound than compound **1-X** (X = Br or Cl), especially towards hydrolysis. Using **Hepta-X$_3$** for C–C coupling reactions can create an inextricable mixture of by-products, as well as solubility issues with the intermediates and final products in organic solvents. Using dissymmetric heptazines bearing long alkyl chains, which make them more soluble and less sensitive than **Hepta-X$_3$** (*e.g.* compound **1-X**), is probably the key to understanding the delicate chemistry of heptazine derivatives.

Focus on Stille coupling

To better understand the impact of the substituent on the outcome of the reaction, we focused on one type of coupling, varying the electronic properties of the substituents. We selected Stille coupling because its tolerance for a wider number of functional groups with superior efficiency compared to other methods makes it a popular choice for highly complex organic syntheses.[42–44] Moreover, the anhydrous conditions required in the procedure to form the organotin compound rule out hydrolysis of **1-Br** as a cause of reaction failure. Although **1-Cl** is known to undergo hydrolysis,[28] aqueous conditions may not be detrimental when cross-coupling is kinetically favored (which is probably the case for the Suzuki coupling producing **2**); however, in the case of less kinetically favourable reaction coupling, **1-Cl** hydrolysis can become the main reaction pathway. This is probably the case for the coupling of less reactive electron-withdrawing substituents where strictly anhydrous conditions are preferable. The results of classical Stille coupling conditions for different aryl substituents are summarised in Table 1.

All couplings with *ortho*-substituted phenyls failed and no trace of the desired compounds was found in either NMR or mass spectrometry analyses. This is due to the well-known steric constraints in Stille coupling reactions.[45,46] The challenging coupling of **1** with nitrophenyl substituents also failed

Table 1 Stille reactions performed with various substituted aryl starting materials

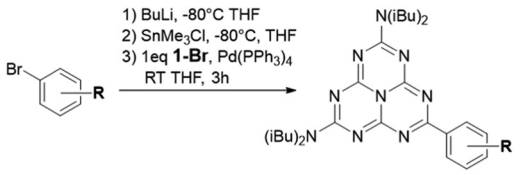

R =	Position	Compound	Organotin[b] (equiv.)	Yield
H	—	**5**	4.4	86%
NO_2	*Meta*	—	1.2	N.d.
	Para	—	1.2	N.d.
CN	*Ortho*	—	1.3	N.d.
	Meta	Not pure[a]	1.3	N.d.
	Para	**7**	1.3	25%
CH_3	*Meta*	Not pure[a]	1.3	N.d.
	Para	**8**	1.2	21%
C_6H_{13}	*Para*	**9**	1.2	45%
OCH_3	*Ortho*	—	2.6	N.d.
	Meta	**10**	1.3	73%
	Para	**6**	2.6	79%

[a] Desired compound detected but not isolated. [b] Used without purification, eq. estimated by NMR. N.d. = not determined.

probably because the nitro group is too strongly deactivating. The only isolable product with an electron-withdrawing substituent is compound **7** which has a cyano group at the *para* position of the phenyl ring and it is obtained in a moderate 25% yield. We observed an increase in the reaction yield as the phenyl substituent's donating properties increased: from 21% for the *para*-methylphenyl compound **8** to 45% for the *para*-hexylphenyl compound **9** and over 70% for the *meta*- or *para*-methoxyphenyl compounds **10** and **6**. While the tris-*para*-anisolyl heptazine was previously obtained *via* the Friedel–Crafts reaction,[31] this newly accessible Stille coupling provides access to the *meta*-position of the methoxy group. However, it should be noted that purification from by-products may prove difficult, particularly with the *meta* position of cyano and methyl groups.

In the literature, Stille coupling is also a classical method to introduce bithiophene bridges in photoactive molecules[47] or to synthesise donor–acceptor copolymers for photovoltaic applications.[48,49] Following the same procedure as before, the coupling of **1–Br** with a bithienyltin compound produced the bithienyl-heptazine compound **11** in 53% yield (see Scheme 3a). In order to expand the functionalization possibilities of these molecules and examine the electronic effects of the heptazine moiety on certain aromatic substituents, we investigated the further reactivity of compounds **5** and **11** (see Scheme 3b). Nitration of the phenylheptazine compound **5** using an excess of nitronium tetrafluoroborate in acetonitrile successfully produced the *meta*-nitrophenylheptazine compound **12** with a yield of 72%. Single crystals suitable for X-ray diffraction were obtained by slowly cooling a saturated solution of **12** in acetonitrile from 50 °C to room temperature (RT). The crystal structure of compound **12** (Fig. 2a) confirms the *meta*-substitution of the nitro group on the aryl ring and the electron-withdrawing character of the heptazine moiety. Compound **12** crystallises in the monoclinic system in the *Pn* space group with one molecule in the asymmetric unit. The three conjugated aromatic rings of the heptazine moiety and the peripheral N atoms remain planar (the average distance of the atoms to the mean plane is 0.056 Å). The mean planes that include the heptazine and the aryl moieties exhibit a slight twist, with a dihedral angle of 5.71(9)° separating them. The nitro group is clearly twisted relative to the aryl ring, forming an angle of 17.2(2)°. The C1–C7 distance of 1.488(5) Å falls within the range of distances reported for heptazine structures with C–C substitutions *via* Friedel–Crafts reactions (from 1.460 to 1.481 Å).[37,38,50] The C11–N10 distance (1.473(5) Å) and the average N10–O distance (1.223(6) Å) fall within the range of distances previously reported for nitrophenyl molecules.[51,52] The molecules are organised into columns along the *a* axis direction with two different heptazine orientations, with π–π stacking occurring between the aryl and the heptazine rings of neighbouring molecules due to the cell translation (Fig. 2b and c). The average plane of the heptazine and the centre of the aryl ring are separated by 3.285(2) Å, indicating a strong π-stacking interaction.[32] The subsequent reduction of the nitro group to an amine in compound **12** could pave the way for the

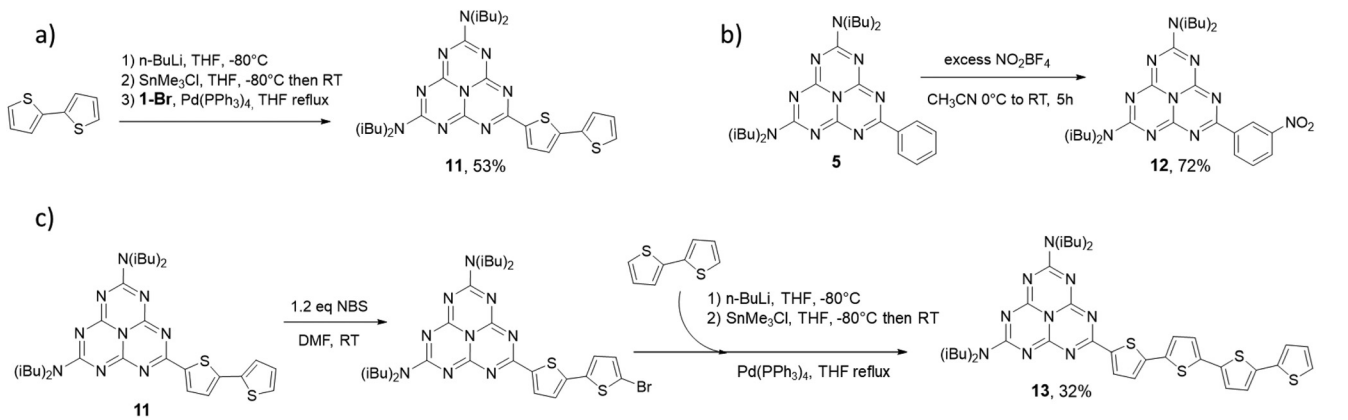

Scheme 3 Syntheses of compounds **11**, **12** and **13**.

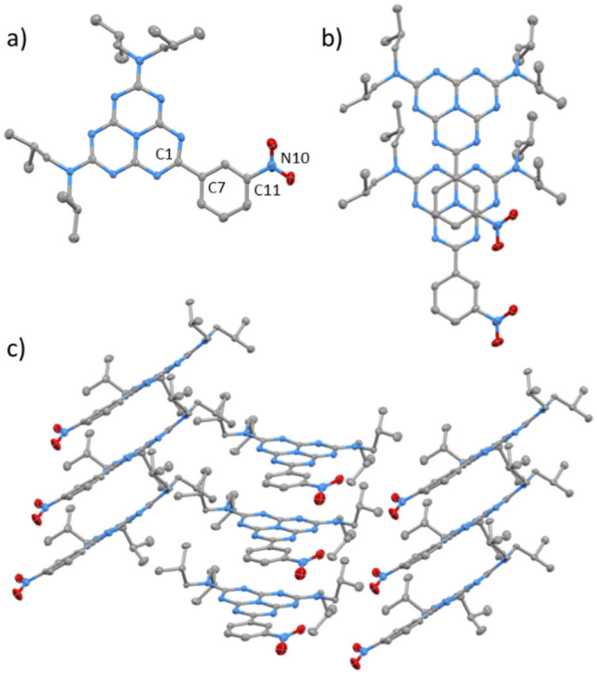

Fig. 2 ORTEP view of the structure of **12**. Ellipsoids at 50% probability. Carbon atoms in grey, nitrogen atoms in blue, and oxygen atoms in red. Hydrogen atoms are omitted for clarity. (a) View of the asymmetric unit, (b) top view of π-stacking, and (c) packing view.

development of more sophisticated heptazine derivatives and efforts to this end are currently ongoing. We then explored using a consecutive Stille reaction in order to increase the thiophene chain size in the bithienyl-heptazine compound **11** (see Scheme 3c). Adding 1.2 eq. of *N*-bromosuccinimide to **11** in dimethylformamide (DMF) at room temperature led to the expected bromination of the terminal thiophene ring. After washing and extraction, the intermediate brominated compound was recovered from the organic phase and used without further purification in a second Stille coupling reaction with the bithienyltin compound. Tetrathienylheptazine **13** was obtained with a global yield of 32%. The compounds **7–13** were characterised using NMR (^{1}H, ^{13}C and 2D techniques), mass spectrometry and FTIR spectroscopy (see the SI). All analyses converge to validate the structure of each molecule. Notably, the FTIR spectrum of **7** shows a characteristic peak at 2230 cm^{-1}, assigned to C≡N stretching vibrations. NMR studies (1D and 2D) of **13** in $CDCl_3$ confirmed the coupling of the two bithiophene units at the α position due to the absence of characteristic signals of β substitution. Moreover, considering the interest in heptazine derivatives for OLED applications, thermogravimetric analysis of compounds **2–13** has also been performed under dinitrogen and the results are available in the SI.

We were interested in comparing the electrochemical and optical properties of this library of heptazine-based compounds bearing novel substituents through C–C bonds to gain fundamental insights. Electrochemistry may provide access to a pseudo LUMO level while absorption and emission properties allow approximation of the HOMO–LUMO gap.

Characterization of the heptazine derivatives

To study the reversibility of the electron transfer in the heptazine derivatives, we examined their behaviour using cyclic voltammetry in DMF under an inert atmosphere. Fig. 3 shows the voltammograms of the first reduction, ordered by redox potential. As expected, compared to the phenyl derivatives (**5** to **10** and **12**), we observed that the reduction potential is more negative for the donor substituents at the *para* position of the phenyl, *i.e.* compounds **6**, **8** and **9**. The most electron-withdrawing substituents, on the other hand, have the least negative potentials (compounds **12** and **7**). On examining thiophene derivatives (compounds **4**, **11** and **13**), it is observed that an increase in the length of the thiophene chain shifts the reduction potential towards more positive values, rendering the compounds easier to reduce. The presence of an additional thiophene in compound **11** makes the first reduction quasi-reversible, as opposed to compound **4**, which is less reversible. Most of the molecules synthesised in this article undergo a quasi-reversible first reduction (except for **3**, which is irreversible) and oxidation waves are inaccessible in the electrochemical window (except for compounds **2** and **13**, see the SI). Heptazine derivatives are mainly obtained by nucleophilic substitution in the literature and possess heptazine–heteroatom bonds. In the rare cases where the electrochemical properties of these heptazine derivatives have been studied, the first reduction event attributed to the heptazine moiety is irreversible,[17,53,54] except in the case of heptazine oligomers (dimers and trimers).[29] There are only two examples in the literature of derivatives fully substituted with aromatic groups linked by C–C bonds to the heptazine unit whose electrochemical properties have been studied. Both systems show a first quasi-reversible reduction.[34,55] Our results confirm that

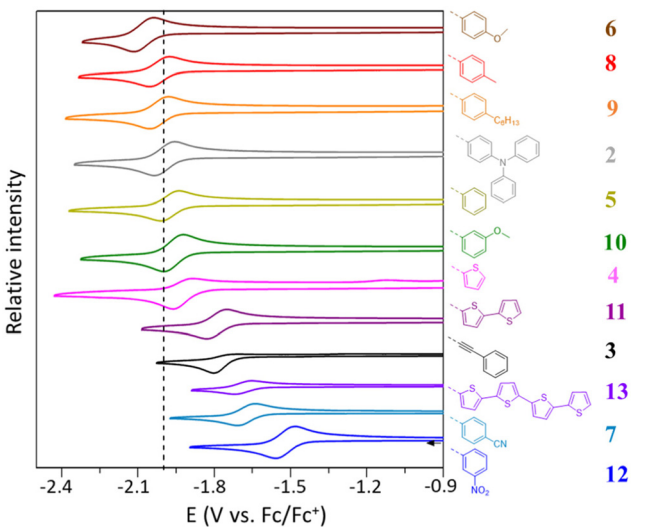

Fig. 3 Cyclic voltammetry under argon of the first reduction event of heptazine derivatives **2–13** (1 mM, 100 mV s^{-1} in DMF + 0.1 M $TBAPF_6$, glassy carbon electrode ∅ = 5 mm) ordered from the most negative to the least negative first reduction potential. The dashed line at −2 V serves as a reference point to facilitate comparison.

the C–C bonds between the aromatic groups and the heptazine platform stabilize the reduced form of the molecule. The reorganisation of electrons and bonds during reduction is diminished, leading to quasi-reversible electron transfer. Increasing the reversibility requires only one aromatic C–C bond in one of the three substitutable positions. All the molecules show a second reduction (below −2 V *versus* Fc/Fc^{+}) which is quasi-reversible for compounds bearing electron-withdrawing groups: **7**, **11**, **12** and **13** (see the SI). For compounds **12** and **13** which have the most positive reduction potentials, a third irreversible reduction can also be seen in the voltammograms. These results are particularly interesting for improving the design of heptazine-based molecules for use in COF, MOF or ligand applications involving electron storage or catalysis.

The optical properties (absorption and emission) of these compounds have been studied in dichloromethane at room temperature. The spectra have been normalised for both absorbance and emission and are shown in Fig. 4 for the phenyl derivatives **5**, **6** and **12** (top), for compound **13** (middle) and for compound **2** (bottom). Absorption and emission spectra of the other compounds, as well as a table including molar extinction coefficients (ε) and Stokes shift calculations, are available in the SI. The phenyl derivatives (compounds **5** to **10** and **12**) all exhibit several absorption bands in the UV region between 268 and 280 nm with high absorption coefficients (ε ranging from 38 000 to 78 000 L mol^{-1} cm^{-1}) which correspond to π–π* transitions. Additionally, two absorption bands are observed around 400 nm (ε, as measured in DMF, is approximately 2000 L mol^{-1} cm^{-1}) which are attributed to n–π* transitions.[29] These n–π* absorption bands are sensitive to the electronic properties of the aromatic substituents. Consequently, they are redshifted in the visible region for compounds bearing electron-withdrawing groups (**7** and **12**). Compounds with anisolyl substituents (**6** and **10**) present an additional absorption band around 320 nm which is likely due to the n–π* transition of the phenoxy doublets. All phenyl derivatives show a similar emission spectrum, regardless of the excitation wavelength, suggesting a comparable relaxation process. It is interesting to note that the emission maximum shifts towards longer wavelengths as the electron-donating properties of the substituents increase, ranging from 425 nm for compound **6** to 460 nm for compounds **7** and **12**. However, the emission intensity varies according to the substituents.

The UV-Vis absorbance spectra of the thiophene derivatives (**4**, **11** and **13**) show two absorption maxima, one of which is common to all three molecules and appears between 260 and 270 nm. Only the monothiophene derivative **4** shows an absorption band around 400 nm, which is common to phenyl derivatives. For compounds **11** and **13**, this n–π* transition is probably hidden under another maximum. Of particular interest is the red shift of this absorption maximum, which increases as the thiophene oligomer length increases. Furthermore, the presence of heptazine improves the charge separation due to its acceptor properties. The absorption maximum of compound **13** (450 nm) is redshifted by almost 80 nm compared to a soluble analogue of the quaterthiophene

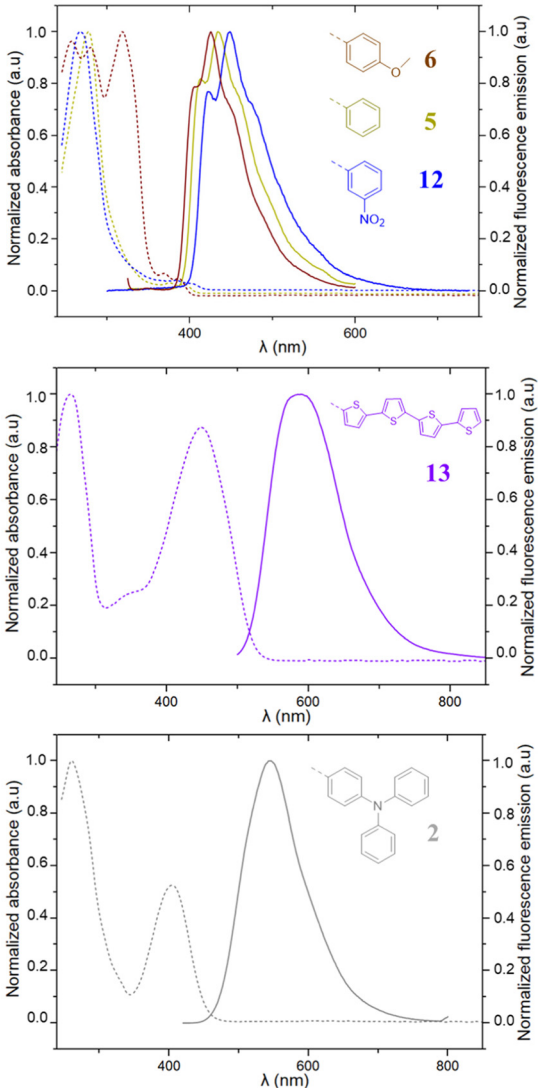

Fig. 4 Normalised absorption (dashed lines) and emission (full lines) in dichloromethane of the phenyl derivatives **5**, **6** and **12** (top), compound **13** (middle) and compound **2** (bottom).

alone in a chlorinated solvent (372 nm).[56] Regarding the fluorescence of these thiophene derivatives, the monothiophene (**4**) shows significantly lower emission intensity than compounds **11** and **13**. Once again, a significant red shift of the emission maximum is observed as the thiophene chain length increases. The emission wavelengths are 440, 456 and 590 nm for compounds **4**, **11** and **13**, respectively.

Finally, compounds **2** and **3** both possess donor groups that differ significantly from the previous derivatives, with a non-planar triphenylamine substituent and a conjugated triple bond, respectively. Compound **3** exhibits two absorption maxima (262 and 282 nm), and a shoulder around 320 nm in its UV region. It also has an absorption edge around 400 nm, which is now characteristic of these heptazine derivatives. Compound **2** exhibits only two absorption maxima, the second of which is shifted towards the visible region (260 and 405 nm). The latter probably masks the absorption edge

around 400 nm. This red shift is due to better charge separation caused by the non-planarity of the triphenylamine substituent, which disrupts electron delocalisation. Regarding their emission spectra, compound **3** is a weak light-emitter, whereas compound **2** exhibits very intense emission with measured quantum yields of 3% and 80%, respectively. The strong emission of **2** is comparable with the HAP-3TPA molecule reported by Adachi *et al.* in 2013.[57] Compound **2** also exhibits the second most red-shifted emission maximum (545 nm) compared to the other derivatives.

Conclusions

This study reports on the functionalisation of heptazine derivatives and describes five types of efficient C–C cross-coupling reactions (Suzuki, Sonogashira, Stille, Kumada and Negishi), all of which were achieved with excellent yields using bromo- and chloro-heptazine precursors. Particular attention was given to Stille coupling, for which the influence of various aromatic organotin reagents on the outcome of the reaction was systematically evaluated. The reactivity of selected aryl and bithiophene derivatives was examined to investigate the electronic behaviour of the heptazine core during nitration, bromination and subsequent cross-coupling steps. In total, twelve heptazine derivatives were synthesised. We analysed their electrochemical properties, as well as their absorption and emission characteristics, revealing a pronounced impact of substituents on the electronic structure and optical responses. Notably, we found that the formation of C–C bonds between the heptazine core and conjugated substituents plays a key role in governing the reversibility of the initial reduction process. Overall, this work is an important step towards developing advanced heptazine-based architectures with potential applications in many different fields.

Conflicts of interest

There are no conflicts to declare.

Data availability

Complementary data for this study are available in the supplementary information (SI). See DOI: **https://doi.org/10.1039/d6qo00267f**.

CCDC 2522075 (**Hepta-Br$_3$**), 2522076 (**1-Br**) and 2522077 (**12**) contain the supplementary crystallographic data for this paper.[58a–c]

Acknowledgements

We thank Dr Murielle Chavarot-Kerlidou and Dr Cyril Aumaître for useful scientific discussions. We thank Yann Kervella for experimental advice and donation of some starting materials. This work is supported by the French National Research Agency in the framework of the "Investissements d'avenir" programs (ANR-15-IDEX-02, CDP-DefiCO2). We are grateful to La Fondation de la Maison de la Chimie who financially supported this study.

References

1 X. Wang, K. Maeda, A. Thomas, K. Takanabe, G. Xin, J. M. Carlsson, K. Domen and M. Antonietti, A metal-free polymeric photocatalyst for hydrogen production from water under visible light, *Nat. Mater.*, 2009, **8**, 76–80.
2 H. Cheng, H. Lv, J. Cheng, L. Wang, X. Wu and H. Xu, Rational Design of Covalent Heptazine Frameworks with Spatially Separated Redox Centers for High-Efficiency Photocatalytic Hydrogen Peroxide Production, *Adv. Mater.*, 2022, **34**, 2107480.
3 Y. Li, Y. Wang, C.-L. Dong, Y.-C. Huang, J. Chen, Z. Zhang, F. Meng, Q. Zhang, Y. Huangfu, D. Zhao, L. Gu and S. Shen, Single-atom nickel terminating sp ^{2} and sp ^{3} nitride in polymeric carbon nitride for visible-light photocatalytic overall water splitting, *Chem. Sci.*, 2021, **12**, 3633–3643.
4 J. Mao, T. Peng, X. Zhang, K. Li, L. Ye and L. Zan, Effect of graphitic carbon nitride microstructures on the activity and selectivity of photocatalytic CO2 reduction under visible light, *Catal. Sci. Technol.*, 2013, **3**, 1253.
5 A. Kumar, P. Kumar, D. Pandey, N. Saini, K. Dhingra, D. Ghosh and K. Kailasam, Molecular engineering of donor–acceptor heptazine-based porous organic polymers for selective photoreduction of CO2 to CO under non-sacrificial conditions in water, *J. Mater. Chem. A*, 2024, **12**, 31244–31252.
6 Y. Deng, T. Sun, S. Zhou, W. Jiang, C. Liu, C. Ma and G. Che, Rational design of a donor–acceptor structure in covalent heptazine frameworks to boost photocatalytic nitrogen fixation, *Chem. Commun.*, 2025, **61**, 3135–3138.
7 H. Wang, S. Wei, M. Li, F. Zhou, J. Li and J. Huang, Rational construction of donor–acceptor covalent heptazine polymers for efficient photocatalytic N2 reduction to NH3, *Chem. Commun.*, 2025, **61**, 19925–19928.
8 N. Aizawa, Y.-J. Pu, Y. Harabuchi, A. Nihonyanagi, R. Ibuka, H. Inuzuka, B. Dhara, Y. Koyama, K. Nakayama, S. Maeda, F. Araoka and D. Miyajima, Delayed fluorescence from inverted singlet and triplet excited states, *Nature*, 2022, **609**, 502–506.
9 J. Li, H. Nomura, H. Miyazaki and C. Adachi, Highly efficient exciplex organic light-emitting diodes incorporating a heptazine derivative as an electron acceptor, *Chem. Commun.*, 2014, **50**, 6174–6176.
10 P. Dad, A. N. Stuart, K. Bergmann, D. M. Mayder, Z. M. Hudson and G. Lakhwani, Impact of Donor Strength on Thermally Activated Delayed Fluorescence in Heptazine-Based Donor–Acceptor Emitters, *J. Phys. Chem. C*, 2025, **129**, 20691–20696.

11 D. Conelli, A. Maggiore, R. Grisorio, G. P. Suranna, V. Maiorano, A. L. Sobolewski, W. Domcke, F. Miomandre and P. Audebert, New Heptazines Bearing Strongly Electron-Donating Substituents with Quasidegenerate Singlet and Triplet Excited States: An Experimental and Computational Study, *J. Phys. Chem. C*, 2025, **129**, 17249–17262.

12 D. Ma, B. Li, Z. Cui, K. Liu, C. Chen, G. Li, J. Hua, B. Ma, Z. Shi and S. Feng, Multifunctional Luminescent Porous Organic Polymer for Selectively Detecting Iron Ions and 1,4-Dioxane via Luminescent Turn-off and Turn-on Sensing, *ACS Appl. Mater. Interfaces*, 2016, **8**, 24097–24103.

13 M. Mohan, S. Rajak, A. A. Tremblay, T. Maris and A. Duong, Syntheses of mono and bimetallic cyamelurate polymers with reversible chromic behaviour, *Dalton Trans.*, 2019, **48**, 7006–7014.

14 M. Mohan, M. Essalhi, D. Durette, L. K. Rana, F. K. Ayevide, T. Maris and A. Duong, A Rational Design of Microporous Nitrogen-Rich Lanthanide Metal–Organic Frameworks for CO2/CH4 Separation, *ACS Appl. Mater. Interfaces*, 2020, **12**, 50619–50627.

15 Y. Yu, Q. Jin, D. Zhu and Y. Ren, Exceptional Lithium-Ion Storage Performance on an Azo-Bridged Covalent Heptazine Framework, *Adv. Funct. Mater.*, 2024, **34**, 2308706.

16 J. Ehrmaier, X. Huang, E. J. Rabe, K. L. Corp, C. W. Schlenker, A. L. Sobolewski and W. Domcke, Molecular Design of Heptazine-Based Photocatalysts: Effect of Substituents on Photocatalytic Efficiency and Photostability, *J. Phys. Chem. A*, 2020, **124**, 3698–3710.

17 L. Galmiche, C. Allain, T. Le, R. Guillot and P. Audebert, Renewing accessible heptazine chemistry: 2,5,8-tris(3,5-diethyl-pyrazolyl)-heptazine, a new highly soluble heptazine derivative with exchangeable groups, and examples of newly derived heptazines and their physical chemistry, *Chem. Sci.*, 2019, **10**, 5513–5518.

18 E. Kroke, M. Schwarz, E. Horath-Bordon, P. Kroll, B. Noll and A. D. Norman, Tri-s-triazine derivatives. Part I. From trichloro-tri-s-triazine to graphitic C3N4 structures, *New J. Chem.*, 2002, **26**, 508–512.

19 J. R. Holst, Doctoral thesis, University of Iowa, 2009.

20 T. J. Koller, K. Witthaut, F. Wolf, J. N. Singer, J. Blahusch, C. Li, V. Valsamidou, D. Johrendt and W. Schnick, Pyrrolation of Melem: A Facile Gateway into the Field of Monomeric s-Heptazine Chemistry, *Chem. – Eur. J.*, 2025, **31**, e202500271.

21 S. M. Sayed, L.-L. Deng, B.-P. Lin and H. Yang, A room-temperature heptazine core discotic liquid crystal, *Liq. Cryst.*, 2017, **44**, 2175–2183.

22 I. Bala, H. Singh, V. R. Battula, S. P. Gupta, J. De, S. Kumar, K. Kailasam and S. K. Pal, Heptazine: an Electron-Deficient Fluorescent Core for Discotic Liquid Crystals, *Chem. – Eur. J.*, 2017, **23**, 14718–14722.

23 C. Posern, U. Böhme, J. Wagler, C.-C. Höhne and E. Kroke, Arylthio- and Arylseleno-Substituted s-Heptazines, *Chem. – Eur. J.*, 2017, **23**, 12510–12518.

24 C. Posern, U. Böhme and E. Kroke, The Reactivity of Cyameluric Chloride C6N7Cl3 towards Phosphines and Phosphine Oxides, *Z. Anorg. Allg. Chem.*, 2018, **644**, 121–126.

25 C.-C. Höhne, C. Posern, U. Böhme, F. Eichler and E. Kroke, Dithiocyanurates and thiocyamelurates: Thermal thiyl radical generators as flame retardants in polypropylene, *Polym. Degrad. Stab.*, 2019, **166**, 17–30.

26 C. Posern, C.-C. Höhne, U. Böhme, C. Vogt and E. Kroke, Synthesis of Thiocyameluric Acid C6N7S3H3, Its Reaction to Alkali Metal Thiocyamelurates and Organic Tris(dithio) cyamelurates, *Chem. – Eur. J.*, 2019, **25**, 15555–15564.

27 A. Schwarzer and E. Kroke, C6N7Cl[N(C6H5)2]2·p-C6H4 $(CH_3)2$—a mono-chloro-tri-s-triazine adduct, *Chem. Commun.*, 2010, **46**, 2829–2831.

28 A. Schwarzer and E. Kroke, 5,8-Bis[bis-(pyridin-2-yl)amino]-1,3,4,6,7,9,9b-hepta-aza-phenalen-2(1H)-one dimethyl sulfoxide monosolvate dihydrate, *Acta Crystallogr., Sect. E: Struct. Rep. Online*, 2014, **70**, o456–o457.

29 A. Zambon, J.-M. Mouesca, C. Gheorghiu, P. A. Bayle, J. Pécaut, M. Claeys-Bruno, S. Gambarelli and L. Dubois, s-Heptazine oligomers: promising structural models for graphitic carbon nitride, *Chem. Sci.*, 2016, **7**, 945–950.

30 H. Schroeder and E. Kober, Some Reactions of Cyameluric Chloride, *J. Org. Chem.*, 1962, **27**, 4262–4266.

31 E. J. Rabe, K. L. Corp, A. L. Sobolewski, W. Domcke and C. W. Schlenker, Proton-Coupled Electron Transfer from Water to a Model Heptazine-Based Molecular Photocatalyst, *J. Phys. Chem. Lett.*, 2018, **9**, 6257–6261.

32 Y. Ke, D. J. Collins, D. Sun and H.-C. Zhou, (10,3)-a Noninterpenetrated Network Built from a Piedfort Ligand Pair, *Inorg. Chem.*, 2006, **45**, 1897–1899.

33 K. Krūkle-Bērziņa, K. Bērziņš and K. Shubin, Synthesis of some heptazine derivatives, *Chem. Heterocycl. Compd.*, 2019, **55**, 1281–1284.

34 D. M. Mayder, R. Hojo, W. L. Primrose, C. M. Tonge and Z. M. Hudson, Heptazine-Based TADF Materials for Nanoparticle-Based Nonlinear Optical Bioimaging, *Adv. Funct. Mater.*, 2022, **32**, 2204087.

35 N. Saini, A. Kumar, B. Kamboj, M. Sachdeva, H. Bhatt, H. N. Ghosh, D. Ghosh and K. Kailasam, Sulfone-Functionalized Covalent Heptazine Polymeric Networks for Selective CO2 Photoreduction in Water: Mechanistic Insights into Sacrificial Donor-Dependent Selectivity, *Adv. Funct. Mater.*, 2025, e20764.

36 R. Guan, A. Shi, X. Zhang, B. Wang, Y. Li and X. Niu, Promoting Heptazine-Based Graphitic Carbon Nitride Photocatalytic Overall Water Splitting by Effectively Assembling Double-Unit Polymers, *ACS Catal.*, 2024, **14**, 18580–18589.

37 D. Chen, W. Chen, G. Zhang, S. Li, W. Chen, G. Xing and L. Chen, N-Rich 2D Heptazine Covalent Organic Frameworks as Efficient Metal-Free Photocatalysts, *ACS Catal.*, 2022, **12**, 616–623.

38 J.-F. Zheng, Z.-P. Xie, Z. Li, Y. Chen, X. Fang, X. Chen and M.-J. Lin, Structural design of small-molecule carbon-

nitride dyes for photocatalytic hydrogen evolution, *Dyes Pigm.*, 2021, **185**, 108946.

39 L. Yin and J. Liebscher, Carbon–Carbon Coupling Reactions Catalyzed by Heterogeneous Palladium Catalysts, *Chem. Rev.*, 2007, **107**, 133–173.

40 V. Farina, V. Krishnamurthy and W. J. Scott, *Organic Reactions*, John Wiley & Sons, Ltd, 2004, pp. 1–652.

41 A. F. Littke and G. C. Fu, Palladium-Catalyzed Coupling Reactions of Aryl Chlorides, *Angew. Chem., Int. Ed.*, 2002, **41**, 4176–4211.

42 K. C. Nicolaou, Y. He, F. Roschangar, N. P. King, D. Vourloumis and T. H. Li, Total synthesis of epothilone E and analogues with modified side chains through the Stille coupling reaction, *Angew. Chem., Int. Ed.*, 1998, **37**, 84–87.

43 C. Cordovilla, C. Bartolomé, J. M. Martínez-Ilarduya and P. Espinet, The Stille Reaction, 38 Years Later, *ACS Catal.*, 2015, **5**, 3040–3053.

44 P. Stanetty, M. Schnürch and M. D. Mihovilovic, Halogenated 2′-Chlorobithiazoles via Pd-Catalyzed Cross-Coupling Reactions, *J. Org. Chem.*, 2006, **71**, 3754–3761.

45 J. delPozo, J. A. Casares and P. Espinet, The decisive role of ligand metathesis in Au/Pd bimetallic catalysis, *Chem. Commun.*, 2013, **49**, 7246–7248.

46 W. Su, S. Urgaonkar, P. A. McLaughlin and J. G. Verkade, Highly Active Palladium Catalysts Supported by Bulky Proazaphosphatrane Ligands for Stille Cross-Coupling: Coupling of Aryl and Vinyl Chlorides, Room Temperature Coupling of Aryl Bromides, Coupling of Aryl Triflates, and Synthesis of Sterically Hindered Biaryls, *J. Am. Chem. Soc.*, 2004, **126**, 16433–16439.

47 J. Zhang, S. Singh, D. K. Hwang, S. Barlow, B. Kippelen and S. R. Marder, 2-Bromo perylene diimide: synthesis using C–H activation and use in the synthesis of bis(perylene diimide)–donor electron-transport materials, *J. Mater. Chem. C*, 2013, **1**, 5093–5100.

48 M. Zhang, X. Guo and Y. Li, Photovoltaic Performance Improvement of D–A Copolymers Containing Bithiazole Acceptor Unit by Using Bithiophene Bridges, *Macromolecules*, 2011, **44**, 8798–8804.

49 C.-H. Chen, C.-H. Hsieh, M. Dubosc, Y.-J. Cheng and C.-S. Hsu, Synthesis and Characterization of Bridged Bithiophene-Based Conjugated Polymers for Photovoltaic Applications: Acceptor Strength and Ternary Blends, *Macromolecules*, 2010, **43**, 697–708.

50 T. Li, B.-T. Liu, Z.-B. Fang, Q. Yin, R. Wang and T.-F. Liu, Integrating active C3N4 moieties in hydrogen-bonded organic frameworks for efficient photocatalysis, *J. Mater. Chem. A*, 2021, **9**, 4687–4691.

51 B. Umamahesh, J. Ajantha, C. Sravani, S. Easwaramoorthi and K. I. Sathiyanarayanan, Luminescent tetrahydrodibenzo[a,i]phenanthridin-5-yl)phenol-boron complexes (borophenanthridines), *Dyes Pigm.*, 2017, **137**, 182–190.

52 I. Medina-Mercado, A. Colin-Molina, J. E. Barquera-Lozada, B. Rodríguez-Molina and S. Porcel, Gold-Catalyzed Ascorbic Acid-Induced Arylative Carbocyclization of Alkynes with Aryldiazonium Tetrafluoroborates, *ACS Catal.*, 2021, **11**, 8968–8977.

53 T. Le, L. Galmiche, G. Masson, C. Allain and P. Audebert, A straightforward synthesis of a new family of molecules: 2,5,8-trialkoxyheptazines. Application to photoredox catalyzed transformations, *Chem. Commun.*, 2020, **56**, 10742–10745.

54 F. Brégier, V. Sol, Y. Champavier, L. Galmiche, C. Allain and P. Audebert, First Example of a Heptazine-Porphyrin Dyad; Synthesis and Spectroscopic Properties, *Molecules*, 2022, **27**, 6698.

55 D. M. Mayder, C. M. Tonge, G. D. Nguyen, R. Hojo, N. R. Paisley, J. Yu, G. Tom, S. A. Burke and Z. M. Hudson, Design of High-Performance Thermally Activated Delayed Fluorescence Emitters Containing s-Triazine and s-Heptazine with Molecular Orbital Visualization by STM, *Chem. Mater.*, 2022, **34**, 2624–2635.

56 G. Bidan, A. De Nicola, V. Enée and S. Guillerez, Synthesis and UV–Visible Properties of Soluble Regioregular Oligo(3-octylthiophenes), Monomer to Hexamer, *Chem. Mater.*, 1998, **10**, 1052–1058.

57 J. Li, T. Nakagawa, J. MacDonald, Q. Zhang, H. Nomura, H. Miyazaki and C. Adachi, Highly Efficient Organic Light-Emitting Diode Based on a Hidden Thermally Activated Delayed Fluorescence Channel in a Heptazine Derivative, *Adv. Mater.*, 2013, **25**, 3319–3323.

58 (*a*) CCDC 2522075: Experimental Crystal Structure Determination, 2026, DOI: **10.5517/ccdc.csd.cc2qnf83**; (*b*) CCDC 2522076: Experimental Crystal Structure Determination, 2026, DOI: **10.5517/ccdc.csd.cc2qnf94**; (*c*) CCDC 2522077: Experimental Crystal Structure Determination, 2026, DOI: **10.5517/ccdc.csd.cc2qnfb5**.